Terahertz emission from laser-driven gas plasmas: A plasmonic point of view

Research Article Vol. 5, No. 12 / December 2018 / Optica 1617

Terahertz emission from laser-driven gas plasmas: a plasmonic point of view

I. Thiele,[1,2,*] B. Zhou,[3] A. Nguyen,[4] E. Smetanina,[5] R. Nuter,[1] K. J. Kaltenecker,[3] P. González de Alaiza Martínez,[1] J. Déchard,[4] L. Bergé,[4] P. U. Jepsen,[3] and S. Skupin[1,6]

[1]Univ. Bordeaux—CNRS—CEA, Centre Lasers Intenses et Applications, UMR 5107, 33405 Talence, France
[2]Department of Physics, Chalmers University of Technology, SE-412 96 Göteborg, Sweden
[3]DTU Fotonik-Department of Photonics Engineering, Technical University of Denmark, DK-2800 Kongens Lyngby, Denmark
[4]CEA/DAM Île-de-France, Bruyères-le-Châtel, 91297 Arpajon, France
[5]Department of Physics, University of Gothenburg, SE-412 96 Göteborg, Sweden
[6]Institut Lumière Matière, UMR 5306 Université Lyon 1—CNRS, Université de Lyon, 69622 Villeurbanne, France
*Corresponding author: illia-thiele@web.de

Received 11 September 2018; revised 19 November 2018; accepted 19 November 2018 (Doc. ID 345671); published 20 December 2018

We disclose an unanticipated link between plasmonics and nonlinear frequency down-conversion in laser-induced gas-plasmas. For two-color femtosecond pump pulses, a plasmonic resonance is shown to broaden the terahertz emission spectra significantly. We identify the resonance as a leaky mode, which contributes to the emission spectra whenever electrons are excited along a direction where the plasma size is smaller than the plasma wavelength. As a direct consequence, such resonances can be controlled by changing the polarization properties of elliptically shaped driving laser pulses. Both experimental results and 3D Maxwell consistent simulations confirm that a significant terahertz pulse shortening and spectral broadening can be achieved by exploiting the transverse driving laser beam shape as an additional degree of freedom.

https://doi.org/10.1364/OPTICA.5.001617

1. INTRODUCTION

Terahertz (THz) radiation has become a ubiquitous tool for many applications in science and technology [1,2]. Quite a number of those applications, for example, THz time-domain spectroscopy, require broadband THz sources. Unlike conventional THz sources such as photo-conductive switches [2] or quantum cascade lasers [3], laser-induced gas plasmas straightforwardly produce emission from THz up to far-infrared frequencies [4]. In the standard setup, a femtosecond (fs) two-color (2C) laser pulse composed of fundamental-harmonic (FH) and second-harmonic (SH) frequency is focused into an initially neutral gas, creating free electrons via tunnel ionization. These electrons are accelerated by the laser electric field and produce a macroscopic current leading to broadband THz emission.

Numerous experimental results show that the laser-induced free electron density has a strong impact on the THz emission spectra [4–8]. While it is frequently observed that a larger free electron density leads to broader THz spectra, the origin of the effect remains controversial. In Refs. [5,7,8], homogeneous plasma oscillations were proposed as an explanation, even though those oscillations are in principle non-radiative [9–16]. Moreover, nonlinear propagation effects have been held responsible for THz spectral broadening as well [6,17].

On the other hand, the gas plasma produced by the fs laser pulse is a finite conducting structure with a lifetime largely exceeding the fs time scale. Thus, one can expect that the gas plasma features plasmonic resonances that may have a significant impact on the THz emission properties [18,19]. However, no direct evidence of plasmonic effects in laser-induced gas plasmas has been observed so far, because it is hard to distinguish them in experiments. Also, from the theoretical point of view, identifying plasmonic effects is not trivial because they require at least a full two-dimensional Maxwell-consistent description. Reduced models like the unidirectional pulse propagation equation [20], which are frequently used to describe plasma-based THz generation [6,8,21], are by construction not capable of capturing such resonant effects.

In this paper, we consider the 2C-laser-induced plasma as a plasmonic structure and investigate under which conditions such a perspective is important. In the context of nanoantennas (or metamaterials), e.g., for SH generation [22], tailoring plasmonic resonances by tuning the shape of the plasmonic particle is a standard approach. Therefore, we follow a similar strategy and modify the usually prolate spheroidal plasma shapes to tri-axial ellipsoids, which can be achieved by using elliptically shaped laser beams. Depending on whether the laser polarization is oriented along the long-beam axis (along y) or along the short-beam axis (along x), plasmonic resonances are triggered or not (see Fig. 1). Because nonlinear propagation effects are in both cases equally present, any difference between the THz emission spectra in these two cases is linked to plasmonic effects. Our experimental results detailed in Section 2 clearly evidence that THz pulses emitted for

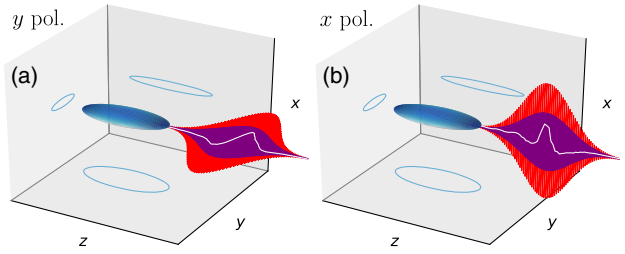

Fig. 1. Illustrated configurations of THz emission from an ellipsoidal plasma induced by a 2C Gaussian laser pulse (FH in red, SH in purple) with strongly elliptical beam shape propagating along z. The laser electric field is (a) y-polarized (along the long axis of the elliptical beam) and (b) x-polarized (along the short axis of the elliptical beam). The plasma is sketched as a blue tri-axial ellipsoid, and its projections are shown in the respective planes. Experimentally measured forward-emitted THz pulses are presented as white lines, demonstrating a significantly shorter pulse duration for an x-polarized pulse, which can be attributed to triggering a plasmonic resonance (see Section 3 for details).

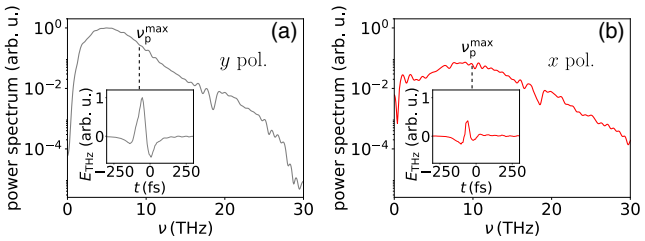

Fig. 2. Experimental THz spectra (see text for details) with (a) a y-polarized laser electric field (along the long axis of the elliptical beam) and (b) an x-polarized laser electric field (along the short axis of the elliptical beam). Corresponding on-axis THz waveforms are shown as insets. The dashed lines specify the estimated maximum plasma frequency.

laser polarization along the short-beam axis are shorter and have a much broader emission spectrum (see Fig. 2). A simple analytical model developed in Section 3 allows us to link this resonant broadening to a leaky mode of the ellipsoidal plasma. In particular, this model shows that the resonance has a strong impact on the spectrum whenever electrons are excited along a direction where the plasma size is smaller than the plasma wavelength. Finally, in Section 4, direct three-dimensional (3D) Maxwell consistent simulations in tightly focused geometry confirm our experimental and theoretical findings.

2. EXPERIMENTAL RESULTS

Experiments are performed in a setup for two-color laser-induced air plasma THz generation and detection sketched in Fig. 3. The laser pulses originate from a 40-fs, 1-kHz Ti:sapphire regenerative laser amplifier. The average laser power through the beam splitter (pump beam) is 230 mW, and the reflected beam (probe beam) has an average power of 200 mW. The pump beam is vertically polarized by a half-wave plate (800 nm) and sent into a 100-μm-thick beta-barium borate (BBO) crystal through a 30-cm focal lens for second-harmonic generation (SHG). The polarization of the fundamental wavelength is then shifted back to horizontal after the SHG process, while the second-harmonic wavelength is kept as horizontally polarized. Off-axis parabolic mirrors are used to collimate and focus the THz field. A piece of high-resistivity

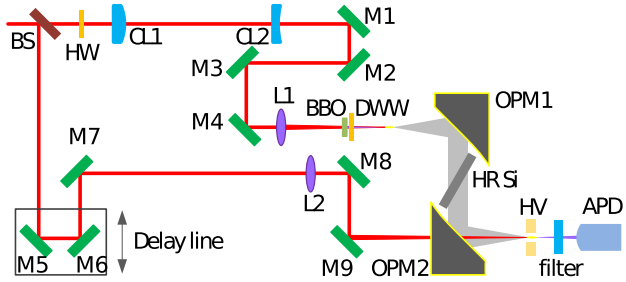

Fig. 3. Sketch for 2C laser-induced air-plasma THz generation and detection system. BS, 800-nm beam splitter; HW, half-wave plate; CL1, plano-convex cylindrical lens, focal length $f = 100$ cm; CL2, plano-concave cylindrical lens, $f = -40$ cm; M1-9, 45 deg incidence high-reflective mirror; Lens L1, $f = 30$ cm; L2, $f = 40$ cm; DWW, dual-wavelength wave plate; OPM1 (OPM2), off-axis parabolic mirrors, reflected focal length, RFL = 10.2 cm (7.6 cm); HR Si, high-resistivity silicon plate, RFL = 7.6 cm; HV, high voltage; APD, Si avalanche photodetector; red line, laser beam; gray area, THz beam.

silicon plate is employed to block the residual FH and SH laser beams. The probe beam, meanwhile, is focused by lens L2 and overlapped with the focus of the THz field through a central hole in the off-axis parabolic mirror (OPM2). The detection of the THz waveform is done by using the so-called air-biased coherent detection scheme [23], where in the presence of the THz field and a high-voltage static field, the four-wave-mixing-generated SH of the probe beam is measured. An avalanche photodiode (APD) is employed as photodetector. A boxcar integrator is then necessary to reshape the fast APD response [few nanoseconds (ns)] before it can be picked up by the lock-in amplifier. The part of the setup where THz waves are involved is covered by a plastic box and purged with dry nitrogen during the measurements in order to avoid water absorption. This setup enables the detection of signals up to 40 THz. A pair of cylindrical lenses is employed in the pump beam arm to elliptically shape the otherwise near-Gaussian pump beam profile. The focal lengths of these lenses have been chosen in such a way that the ratio of the transverse extensions of the plasma is expected to be about 2.5. We rotate both cylindrical lenses by 90° to switch the pump electric field polarization with respect to the elliptically shaped beam and plasma profile. The probe beam arm, on the other hand, is kept the same to ensure identical probe conditions for THz waveforms generated by different pump beam modes.

The experimental 2C elliptical beam creates an about 2.5-cm-long plasma for any rotation angle of the cylindrical lenses. We report no visible difference of the plasmas created in all the configurations. To obtain more details about the ellipsoidal electron density profile under the present experimental conditions, we performed simulations with the unidirectional pulse propagation equation (UPPE) approach [20]. As can be seen in Fig. 4(a), the laser beam is focused after about 5 cm. In agreement with the experimental observations, the 230-μJ laser pulse creates a 2.5-cm-long plasma [see Fig. 4(a)]. The peak electron density grows to $n_e^{max} = 1.2 \times 10^{18}$ cm^{-3}, which corresponds to the maximum plasma frequency $\nu_p^{max} = \sqrt{q_e^2 n_e^{max}/(m_e \epsilon_0)}/(2\pi) = 9.9$ THz and the minimum plasma wavelength $\lambda_p^{min} = 30$ μm. The transverse plasma shape at the focus is strongly elliptical [see Fig. 4(b)]. The transverse FWHM extensions of the elliptical plasma were estimated as 20 μm and 54 μm, giving a ratio of the

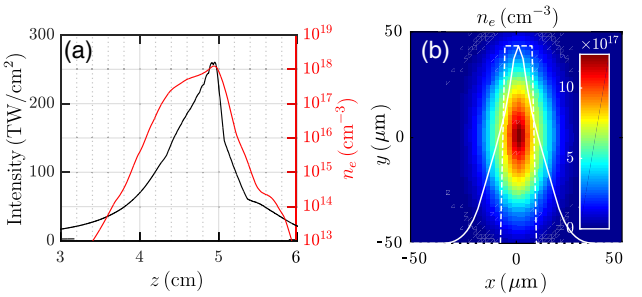

Fig. 4. Results of the UPPE simulation: (a) maximum intensity (black line) and electron density (red line) in the transverse plane and in time along the propagation axis z; (b) electron density profile in the (x, y) plane at the nonlinear focus $z \simeq 5$ cm. The line-out of the profile along $y = 0$ is presented as a solid white line. The approximation for the plasma slab model is sketched as a dashed white line.

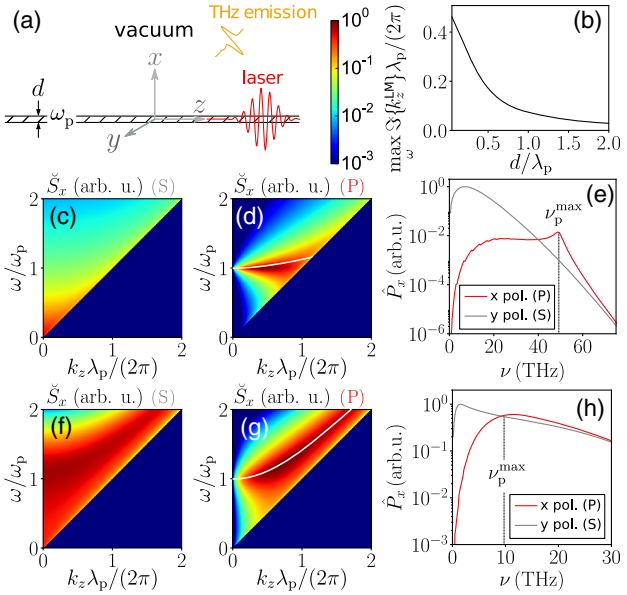

Fig. 5. (a) Illustration of the plasma slab model. (b) Imaginary part $\Im\{k_z^{LM}\}$ of the leaky mode propagation constant versus the slab thickness d in P polarization. Transverse Poynting flux for a δ excitation (see text for details) for (c) S and (d) P polarization. In (d), the real part $\Re\{k_z^{LM}\}$ of the leaky mode propagation constant is indicated by a white line. (e) Far-field spectra for S and P polarization predicted by the plasma slab model employing source terms obtained from 2D paraxial laser field propagation, reproducing well the 2D and 3D simulation results from Fig. 8. The slab thickness is $d = 0.4$ μm, and the plasma frequency is $\omega_p/(2\pi) = \nu_p = 49.15$ THz. (f)–(h) Same as (c)–(e), but for $d = 15$ μm and $\nu_p = 10$ THz, reproducing well the experimental results from Fig. 2.

transverse extensions of the plasma of 2.7, which is close to the expected value. Thus, λ_p^{min} is smaller than the plasma size in one direction and larger in the other direction, which turn out to be the proper conditions to observe a significant difference in the THz emission spectra (see Section 3).

The detected angularly integrated THz spectra and waveforms are presented in Fig. 2. The FWHM THz pulse duration for x polarization is about 1.6 times shorter than for y polarization. A pyroelectric measurement with a detection bandwidth limited to 12 THz revealed a THz pulse energy ratio between y polarization and x polarization of 2.5. The spectrum for x polarization is significantly broader than for y polarization. Moreover, the maximum THz emission for x polarization is found near the estimated maximum plasma frequency (dashed line). Note that the spectral feature around 18 THz is the phonon band absorption of the high-resistivity silicon plate, which is used between the two off-axis parabolic mirrors to block the pump and second-harmonic wavelengths.

3. THEORETICAL EXPLANATION

In the following, we want to explain the difference in the THz emission spectra between the y polarization (laser electric field polarized along the long-beam axis) and x polarization (laser electric field polarized along the short-beam axis). To this end, we resort to a reduced model before solving the full Maxwell-consistent problem in Section 4.

For 2C-driving laser pulses and laser intensities of 10^{14}–10^{16} W/cm^2, the ionization current (IC) mechanism is responsible for THz generation in gas plasmas [4]. Thus, the THz-emitting current $\mathbf{J}$ is given by

$$\partial_t \mathbf{J} + \nu_{ei}\mathbf{J} = \frac{q_e^2}{m_e} n_e \mathbf{E}, \tag{1}$$

with electron charge q_e, mass m_e, and electric field $\mathbf{E}$. The electron density n_e is computed by means of rate equations employing a tunnel ionization rate [24,25], and the electron-ion collision frequency ν_{ei} depends on the ion densities and the electron energy density [26]. Equation (1) coupled to Maxwell's equations also appears as the lowest order of the expansion developed in [12] and fully comprises the IC mechanism [27].

Our reduced model requires three major approximations. First, we assume translational invariance in the y direction and solve a two-dimensional (2D) problem in x and z only. This means that the major axis of our elliptical beams is now infinite. The second major assumption concerns Eq. (1). The main nonlinearity appears due to the product of the time-dependent electron density n_e and electric field $\mathbf{E}$. We split the electric field according to $\mathbf{E} = \tilde{\mathbf{E}} + \mathbf{E}_L$, where $\tilde{\mathbf{E}}$ is the field due to interaction of the laser with the plasma and $\mathbf{E}_L$ is the laser field defined by its 2D propagation in vacuum. For a qualitative understanding of the phenomenon it is sufficient to assume the paraxial solution for the laser electric field $\mathbf{E}_L$. Then, the right-hand side of Eq. (1) reads $\frac{q_e^2}{m_e} n_e \tilde{\mathbf{E}} + \frac{q_e^2}{m_e} n_e \mathbf{E}_L$. An additional simplification, which allows further analytical treatment, is to replace in the first term the time-dependent electron density $n_e(t)$ by a time-invariant electron density n_0, but keep $n_e(t)$ in the second term (THz current source) accounting for ionization by the laser. By doing so, we consider a plasma with electron density n_0 to be excited by the current source $\iota = \frac{q_e^2}{m_e} n_e \mathbf{E}_L$. The third assumption is finally to consider a plasma slab of thickness d as sketched in Fig. 5(a) with translational invariance in y and z. Above and below the slab we assume a semi-infinite vacuum. For the time-invariant electron density in the slab we choose the overall peak density n_e^{max}, and we can write

$$n_0 = n_e^{max}\theta(x - d/2)\theta(d/2 - x), \tag{2}$$

where θ denotes the usual step or Heaviside function.

Let us first discuss the response of such a plasma slab and solve the reflection transmission problem for an incident plane wave in the x, z plane. In the context of a reflection transmission problem,

the y-polarized electric field configuration is often called S polarization, and the x-polarized configuration is referred to as P polarization; the S-polarization mode governs the B_x, E_y, B_z components, and the P-polarization mode the E_x, B_y, E_z components of the electromagnetic field.

For the sake of simplicity, we neglect losses in the slab and set $\nu_{ei} = 0$. The reflectivity for S and P polarization reads (see Supplement 1 for details)

$$\rho_{S/P} = \left| \frac{\Lambda^{v2} - \Lambda^{p2}\alpha_{S/P}^2}{\Lambda^{v2} + \Lambda^{p2}\alpha_{S/P}^2 + \frac{2\Lambda^v\Lambda^p\alpha_{S/P}}{\tanh(\Lambda^p d)}} \right|^2, \tag{3}$$

with $\Lambda^v = \sqrt{k_z^2 - \omega^2/c^2}$, $\Lambda^p = \sqrt{k_z^2 - \epsilon^p\omega^2/c^2}$, $\alpha_S = 1$, $\alpha_p = 1/\epsilon^p$, and plasma dispersion $\epsilon^p = 1 - \omega_p^2/\omega^2$. Singularities of the reflectivity correspond to guided modes, and it is known that for frequencies below the plasma frequency ω_p two surface plasmon polaritons (SPPs) exist for P polarization [28]. Their real propagation constants k_z^{SPP} are zeros of the denominator of Eq. (3). For S polarization, no such guided modes exist. What turns out to be very relevant for the following analysis is that for P polarization the plasma slab also features a *leaky mode* slightly above the plasma frequency ω_p. A leaky mode solution has a complex propagation constant k_z^{LM}. It features a Poynting flux away from the guiding structure, in our case the plasma slab, and its amplitude decreases exponentially upon propagation in the z direction, which is why it is termed *leaky*.

The leaky mode is naturally coupled to the radiative field and can represent a solution of the driven system with the source [19,29–31]. In order to find the leaky mode for the plasma slab, one has to substitute $\Lambda^v \to -\Lambda^v$ in Eq. (3), that is, switch the Poynting flux in the vacuum away from the slab, and look for complex zeros of the denominator as follows:

$$\tanh(\Lambda^p d) = \frac{2\Lambda^v\Lambda^p\epsilon^p}{\Lambda^{v2}\epsilon^{p2} + \Lambda^{p2}}. \tag{4}$$

For given frequency ω and thickness d, the imaginary part $\Im\{k_z^{LM}\}$ of the complex solution to Eq. (4) determines how strong radiation *leaks* from the plasma slab to the surrounding vacuum. In Fig. 5(b), the maximum of $\Im\{k_z^{LM}\}$ versus the slab thickness d is shown, clearly indicating that only for thin plasma slabs ($d < \lambda_p$) the leaky mode should play a role in the emission spectrum.

Let us now examine the response of the plasma slab to a δ excitation $\iota \propto \delta(z)\delta(t)$ for $|x| < d/2$ along y (S) and x (P). Such excitation is constant in the ω, k_z Fourier domain. To collect the emission radiating from the slab, we consider the x component of the spectral Poynting flux $\breve{S}_x \propto \Re\{\breve{\mathbf{E}} \times \breve{\mathbf{B}}^\star\}_x$ through two planes normal to the x axis situated above and below the slab. In Figs. 5(c) and 5(d), $\breve{S}_x$ is visualized for a thin slab $d = 0.066\lambda_p$. The resonant emission following the real part $\Re\{k_z^{LM}\}$ of the leaky mode for x polarization (white line) is evident. For the larger slab with $d = 0.5\lambda_p$ shown in Figs. 5(f) and 5(g), the resonance associated with the leaky mode moves away from ω_p.

In order to make a more quantitative comparison with previous experiments and upcoming simulation results, we now approximate the source term ι by 2D paraxial laser field propagation and the corresponding time- and z-dependent electron density on the optical axis. The electric field on the optical axis in quasi-monochromatic 2D paraxial approximation reads

$$\mathbf{E}_L(z,t) \approx \Re\left\{ \frac{E_\omega e^{-\frac{(t-z/c)^2}{t_0^2} - i\omega_L(t-z/c)}}{\sqrt{1 + i\frac{z}{z_R(\omega_L)}}} \right\}\mathbf{e}_L + \Re\left\{ \frac{E_{2\omega} e^{-\frac{(t-z/c)^2}{t_0^2} - i2\omega_L(t-z/c) - i\varphi}}{\sqrt{1 + i\frac{z}{z_R(2\omega_L)}}} \right\}\mathbf{e}_L, \tag{5}$$

where E_ω, $E_{2\omega}$ are the FH or SH electric field amplitudes, t_0 is the $1/e$ pulse duration, $\omega_L = 2\pi c/\lambda_L$ is the FH laser frequency with wavelength λ_L, φ is the relative phase angle between FH and SH, the unit vector $\mathbf{e}_L$ defines the (linear) laser polarization direction, $z_R(\omega) = w_{0,x}^2\omega/2c$ is the Rayleigh length, and the symbol $\Re$ denotes the real part of a complex quantity. Then the model current source in the slab reads

$$\iota = \frac{q_e^2 n_e[\mathbf{E}_L]}{m_e}\mathbf{E}_L. \tag{6}$$

As before, we assume ι to be invariant along x inside the slab and zero outside for simplicity. The current source for a tightly focused configuration is displayed in Fig. 6(a). In this case, the excitation leads to slightly forward oriented THz emission. The excitation spectrum for a weakly focused beam is presented in Fig. 6(b). Here, the excitations happen close to the vacuum light line $k_z(\omega) = \omega/c$. As the result, THz waves are emitted rather in a forward cone.

Corresponding angularly integrated far-field power spectra $\hat{P}_x$ for the 2D plasma slab model are shown in Figs. 5(e) and 5(h). The resulting THz emission spectra in Fig. 5(h) reproduce well the qualitative behavior of the experimental spectra in Fig. 2; in contrast to y polarization (S), the emission spectrum for x polarization (P) is broadened around the maximum plasma frequency ν_p^{max}. For the thinner slab and higher plasma frequency in Fig. 5(e), which rather mimics the situation of the upcoming simulations, the resonance peak in the spectrum for x polarization is

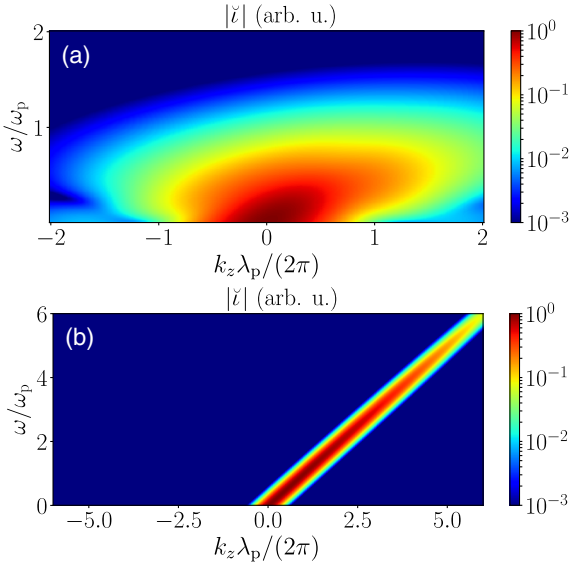

Fig. 6. Excitation source terms, which are used to model the THz emission spectra presented in Figs. 5(e) and 5(h): (a) strongly focused configuration leading to a thin plasma and (b) weakly focused configuration leading to a thicker plasma.

stronger and less broad, as expected from the behavior of the leaky mode.

Before continuing with full Maxwell-consistent simulation results, let us give an intuitive explanation for the difference in the THz spectra in the low-frequency range well below ν_p. When the plasma current is excited along the invariant y direction, no charge separation occurs due to the displacement of the electrons with respect to the ions. Thus, there is no restoring force and low-frequency currents can persist and emit radiation. In contrast, when the plasma current is excited along the x direction with strong plasma gradients, a significant charge separation force pulls the electrons back to the ions, which prevents the generation of low-frequency currents. In 3D this scenario also holds: the charge separation effects are more pronounced for laser polarization along the short-beam axis, which explains the smaller THz signal in the lower frequency range in experiments and simulations for this case [see Figs. 2 and 8].

4. MAXWELL-CONSISTENT MODELING

In the following, we consider the results of full Maxwell-consistent simulations obtained with the code ARCTIC [27]. Here, the electron density is space- and time-dependent, and the electric field is treated self-consistently by coupling the complete current Eq. (1) to the Maxwell's equations. Maxwell-consistent simulations are computationally expensive, and modeling the experimental configuration with centimeter (cm)-long gas plasmas is beyond the possibilities of current supercomputer clusters. In contrast, when focusing the laser pulse strongly, the gas plasma can be only tens-of-micrometers (μm) long and less than 1 μm thick [27]. As can be anticipated from Fig. 5, the small transverse size is favorable to excite a leaky mode for the x-polarized laser case.

We define the driving laser pulse by prescribing its transverse vacuum electric field at focus as

$$\mathbf{E}_{\mathrm{L},\perp}(\mathbf{r}_\perp, z=0, t) = \exp\left(-\frac{x^2}{w_{0,x}^2} - \frac{y^2}{w_{0,y}^2} - \frac{t^2}{t_0^2}\right) \times [E_\omega \cos(\omega_\mathrm{L} t) + E_{2\omega} \cos(2\omega_\mathrm{L} t + \varphi)]\mathbf{e}_\mathrm{L}, \tag{7}$$

where $w_{0,x}$ is the short and $w_{0,y}$ is the long vacuum focal beam width. The laser pulse propagates in the positive z direction, and the origin of the coordinate system is at the vacuum focal point. By defining the tightly focused laser pulse at the vacuum focus, we follow the algorithm described in [32].

The laser pulse parameters are chosen such that in argon with initial neutral density $n_a = 3 \times 10^{19}$ cm^{-3} (≈1 bar) a fully singly ionized ellipsoidal plasma is created (see Supplement 1 for details). The peak electron density $n_e^{\max} = n_a$ translates into a maximum plasma frequency $\nu_p^{\max} = \sqrt{q_e^2 n_a/(m_e \epsilon_0)}/(2\pi) \approx 50$ THz and a minimum plasma wavelength $\lambda_p^{\min} = c/\nu_p^{\max} \approx 6$ μm. As visualized in Fig. 7, the transverse plasma profile is strongly elliptical, that is, along the x direction the plasma size is less than 1 μm, whereas along the y direction the plasma is approximately 10 μm wide. By setting the linear laser polarization $\mathbf{e}_\mathrm{L} = \mathbf{e}_y$ or $\mathbf{e}_\mathrm{L} = \mathbf{e}_x$, we thus excite a THz-emitting current $\mathbf{J}$ along the y direction where the plasma profile is wide or along the x direction where the plasma profile is narrow.

Considering the forward-emitted THz radiation in Fig. 8, we find strong single-cycle pulses reaching field amplitudes

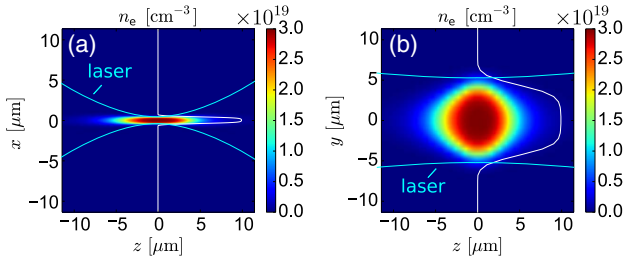

Fig. 7. Electron density in the (a) zx and (b) yz planes after ionization of an argon gas with initial neutral density $n_a = 3 \times 10^{19}$ cm^{-3} (≈1 bar) by a 2C elliptically shaped laser pulse ($E_\omega = 40$ GV/m, $E_{2\omega} = 20$ GV/m, $t_0 = 50$ fs, $w_{0,x} = \lambda_{\mathrm{FH}} = 0.8$ μm, $w_{0,y} = 8$ μm). The respective electron density profiles at focus ($z = 0$) are visualized by the bright white lines. The waist of the focused laser is tracked by the light blue lines.

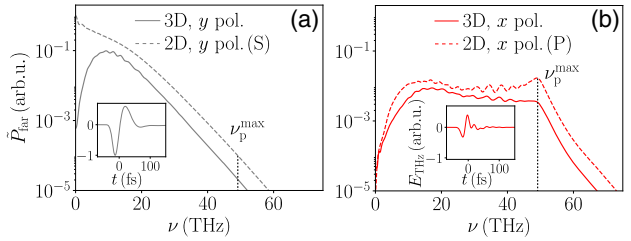

Fig. 8. Angularly integrated far-field spectra for the elliptical beams from Fig. 7 (solid lines) and corresponding results from 2D simulations assuming translational invariance in y (dashed lines). The insets show the forward-emitted THz pulses recorded at $z = 12.7$ μm behind the plasma.

of 10 kV/cm. Most importantly, the THz pulse obtained for x polarization (b) is two times shorter than for y polarization (a), as a direct consequence of the THz emission spectra that are dramatically different. 3D angularly integrated THz far-field spectra in Fig. 8 reveal that for x polarization the THz spectrum is broadened up to about 50 THz and the maximum plasma frequency $\nu_p^{\max}$, while for y polarization no such broadening is found. The total THz pulse energy ($\nu < 70$ THz) for y polarization is 4.8 times larger than for x polarization.

The dashed lines in Fig. 8 show the results of the corresponding 2D simulations, i.e., $w_{0,y} \to \infty$. In this limit, we find a similar behavior: no broadening if the laser electric field is oriented in the now translationally invariant y direction (involving B_x, E_y, B_z, S polarization), and broadening up to $\nu_p^{\max}$ if the laser electric field points in the x direction (involving E_x, B_y, E_z, P polarization) where the plasma profile is narrow. This observation additionally justifies our restriction to 2D for our theoretical model in the previous section. Note that any other polarization state in 2D geometry can be written as the superposition of these two cases, provided that the plasma density remains unchanged. We checked that this property also holds for 3D elliptical beams (see Supplement 1 for details). This possibility of superposing the x and y polarizations implies that the THz emission spectrum can be tuned by rotating the linear polarization of the incoming laser pulse.

5. CONCLUSION

In summary, we have shown that plasmonic effects can significantly broaden the terahertz emission spectrum from femtosec-

ond-laser-induced gas plasmas when the corresponding plasma wavelengths are larger than the transverse plasma size. In the framework of a simplified model considering a plasma slab, we identified the plasmonic resonance responsible for the observed spectral features as a leaky mode. Our model seems to be predictive in a microplasma configuration as well as for larger plasmas, as they are employed in standard two-color setups for THz generation. We propose an efficient THz-generation scheme to access this effect by two-color elliptically shaped laser-beam-induced gas plasmas via the ionization current mechanism and demonstrate its experimental feasibility. By turning the polarization of the excitation through adjusting the linear laser polarization, we can switch THz spectral broadening due to plasmonic resonances on or off and thus control the THz emission spectrum. We believe that considering the gas plasma as a THz plasmonic particle paves the way towards active resonant control of THz generation and will trigger further experimental and theoretical efforts in this direction.

Funding. National Priorities Research Program, Qatar National Research Fund (QNRF) (NPRP 8-246-1- 060); Projet ALTESSE, Agence Nationale de la Recherche (ANR); Knut och Alice Wallenbergs Stiftelse; Mésocentre de Calcul Intensif Aquitaine (MCIA); Grand Équipement National pour le Calcul Intensif (GENCI) (A0040507594, A0030506129); Swedish National Infrastructure for Computing (SNIC) (SNIC2018-4-12, SNIC-2017-1-484, SNIC2018-4-38).

See Supplement 1 for supporting content.

REFERENCES AND NOTES

1. T. Kampfrath, K. Tanaka, and K. A. Nelson, "Resonant and nonresonant control over matter and light by intense terahertz transients," Nat. Photonics **7**, 680–690 (2013).
2. M. Tonouchi, "Cutting-edge terahertz technology," Nat. Photonics **1**, 97–105 (2007).
3. M. S. Vitiello, G. Scalari, B. Williams, and P. D. Natale, "Quantum cascade lasers: 20 years of challenges," Opt. Express **23**, 5167–5182 (2015).
4. K. Y. Kim, A. J. Taylor, S. L. Chin, and G. Rodriguez, "Coherent control of terahertz supercontinuum generation in ultrafast laser-gas interactions," Nat. Photonics **2**, 605–609 (2008).
5. H. Hamster, A. Sullivan, S. Gordon, and R. W. Falcone, "Short-pulse terahertz radiation from high-intensity-laser-produced plasmas," Phys. Rev. E **49**, 671–677 (1994).
6. I. Babushkin, W. Kuehn, C. Köhler, S. Skupin, L. Bergé, K. Reimann, M. Woerner, J. Herrmann, and T. Elsaesser, "Ultrafast spatiotemporal dynamics of terahertz generation by ionizing two-color femtosecond pulses in gases," Phys. Rev. Lett. **105**, 053903 (2010).
7. N. Li, Y. Bai, T. Miao, P. Liu, R. Li, and Z. Xu, "Revealing plasma oscillation in THz spectrum from laser plasma of molecular jet," Opt. Express **24**, 23009–23017 (2016).
8. V. A. Andreeva, O. G. Kosareva, N. A. Panov, D. E. Shipilo, P. M. Solyankin, M. N. Esaulkov, P. González de Alaiza Martínez, A. P. Shkurinov, V. A. Makarov, L. Bergé, and S. L. Chin, "Ultrabroad terahertz spectrum generation from an air-based filament plasma," Phys. Rev. Lett. **116**, 063902 (2016).
9. V. T. Tikhonchuk, "Comment on 'Generation of electromagnetic pulses from plasma channels induced by femtosecond light strings'," Phys. Rev. Lett. **89**, 209301 (2002).
10. A. M. Bystrov, N. V. Vvedenskii, and V. B. Gildenburg, "Generation of terahertz radiation upon the optical breakdown of a gas," J. Exp. Theor. Phys. Lett. **82**, 753–757 (2005).
11. V. B. Gildenburg and N. V. Vvedenskii, "Optical-to-THz wave conversion via excitation of plasma oscillations in the tunneling-ionization process," Phys. Rev. Lett. **98**, 245002 (2007).
12. I. Thiele, R. Nuter, B. Bousquet, V. Tikhonchuk, S. Skupin, X. Davoine, L. Gremillet, and L. Bergé, "Theory of terahertz emission from femtosecond-laser-induced microplasmas," Phys. Rev. E **94**, 063202 (2016).
13. P. Sprangle, J. R. Peñano, B. Hafizi, and C. A. Kapetanakos, "Ultrashort laser pulses and electromagnetic pulse generation in air and on dielectric surfaces," Phys. Rev. E **69**, 066415 (2004).
14. L. M. Gorbunov and A. A. Frolov, "Transition radiation generated by a short laser pulse at a plasma-vacuum interface," Plasma Phys. Rep. **32**, 850–865 (2006).
15. P. González de Alaiza Martínez, X. Davoine, A. Debayle, L. Gremillet, and L. Bergé, "Terahertz radiation driven by two-color laser pulses at near-relativistic intensities: competition between photoionization and Wakefield effects," Sci. Rep. **6**, 26743 (2016).
16. C. Miao, J. P. Palastro, and T. M. Antonsen, "Laser pulse driven terahertz generation via resonant transition radiation in inhomogeneous plasmas," Phys. Plasmas **23**, 063103 (2016).
17. E. Cabrera-Granado, Y. Chen, I. Babushkin, L. Bergé, and S. Skupin, "Spectral self-action of THz emission from ionizing two-color laser pulses in gases," New J. Phys. **17**, 023060 (2015).
18. V. A. Kostin and N. V. Vvedenskii, "Ionization-induced conversion of ultrashort Bessel beam to terahertz pulse," Opt. Lett. **35**, 247–249 (2010).
19. V. A. Kostin and N. V. Vvedenskii, "DC to AC field conversion due to leaky-wave excitation in a plasma slab behind an ionization front," New J. Phys. **17**, 033029 (2015).
20. M. Kolesik and J. V. Moloney, "Nonlinear optical pulse propagation simulation: from Maxwell's to unidirectional equations," Phys. Rev. E **70**, 036604 (2004).
21. I. Dey, K. Jana, V. Fedorov, A. Koulouklidis, A. Mondal, M. Shaikh, D. Sarkar, A. Lad, S. Tzortzakis, A. Couairon, and G. Kumar, "Highly efficient broadband terahertz generation from ultrashort laser filamentation in liquids," Nat. Commun. **8**, 1184 (2017).
22. S. B. Hasan, C. Etrich, R. Filter, C. Rockstuhl, and F. Lederer, "Enhancing the nonlinear response of plasmonic nanowire antennas by engineering their terminations," Phys. Rev. B **88**, 205125 (2013).
23. J. Dai, X. Xie, and X.-C. Zhang, "Detection of broadband terahertz waves with a laser-induced plasma in gases," Phys. Rev. Lett. **97**, 103903 (2006).
24. M. Ammosov, N. Delone, and V. Krainov, "Tunnel ionization of complex atoms and of atomic ions in an alternating electric field," Sov. Phys. JETP **64**, 1191–1194 (1986).
25. G. L. Yudin and M. Y. Ivanov, "Nonadiabatic tunnel ionization: looking inside a laser cycle," Phys. Rev. A **64**, 013409 (2001).
26. J. D. Huba, *NRL Plasma Formulary* (Naval Research Laboratory, 2013).
27. I. Thiele, P. González de Alaiza Martínez, R. Nuter, A. Nguyen, L. Bergé, and S. Skupin, "Broadband terahertz emission from two-color femtosecond-laser-induced microplasmas," Phys. Rev. A **96**, 053814 (2017).
28. P. Berini, "Long-range surface plasmon polaritons," Adv. Opt. Photon. **1**, 484–588 (2009).
29. N. Marcuvitz, "On field representations in terms of leaky modes or eigenmodes," IRE Trans. Antennas Propag. **4**, 192–194 (1956).
30. L. Goldstone and A. Oliner, "Leaky-wave antennas I: rectangular waveguides," IRE Trans. Antennas Propag. **7**, 307–319 (1959).
31. J. Hu and C. R. Menyuk, "Understanding leaky modes: slab waveguide revisited," Adv. Opt. Photon. **1**, 58–106 (2009).
32. I. Thiele, S. Skupin, and R. Nuter, "Boundary conditions for arbitrarily shaped and tightly focused laser pulses in electromagnetic codes," J. Comput. Phys. **321**, 1110–1119 (2016).